International Journal of Microwave and Wireless Technologies

cambridge.org/mrf

Centimeter-wave passive electronically scanned array using movable short phase shifters

Mostafa O. Shady[1], Mohamed Mamdouh M. Ali[2], Syed M. Sifat[3], Khelifa Hettak[4], Larbi Talbi[4] and Ke Wu[5]

[1]R&D Department, Scientific Microwave Corporation, Montreal, QC, Canada; [2]Department of Electrical Engineering, Faculty of Engineering, Assiut University, Assiut, Egypt; [3]Department of Electrical, Computer, and Biomedical Engineering, Toronto Metropolitan University, Toronto, ON, Canada; [4]Department of Electrical and Computer Engineering, Université du Québec en Outaouais, Gatineau, QC, Canada and [5]Department of Electrical Engineering, Polytechnique Montreal, Montreal, QC, Canada

Research Paper

Cite this article: Shady MO, Ali MMM, Sifat SM, Hettak K, Talbi L, Wu K (2026) Centimeter-wave passive electronically scanned array using movable short phase shifters. *International Journal of Microwave and Wireless Technologies* **18**(3), 384–393. https://doi.org/10.1017/S1759078726103304

Received: 29 September 2025
Revised: 24 April 2026
Accepted: 30 April 2026
First published online: 29 May 2026

Keywords:
centimeter-wave; high-power; phased array; reconfigurable phase shifter; rectangular waveguide

Corresponding author: Mostafa O. Shady; Email: mostafashady@live.co.uk

Abstract

This paper proposes an electronically controlled reconfigurable scanned array that uses movable short phase shifters suitable for 6G applications. Excellent performance is demonstrated by the passive electronically scanned array (PESA) operating in the centimeter-wave frequency region (13–17 GHz). Four digitally controlled variable reflect-type phase shifters, each built with a 90° hybrid coupler with a movable short circuit, are integrated with a 2×2 horn antenna array. The assembly also has E–H feeding networks, which help the antenna array receive a uniform signal distribution. Outstanding performance is demonstrated and verified by time and frequency domain simulation results of the full PESA, which show continuous main-lobe scanning in the azimuth and elevation planes. Over the operating bandwidth, the proposed PESA maintains a steady gain of 14 ± 2 dBi while achieving a matching level below −12 dB.

Introduction

An earlier version of this paper was presented at the 19th Conference of Antennas and Propagation (EuCAP 2025) and was published in its Proceedings [1].

Wireless networks are now dynamic platforms with excellent signal integrity, secure connections, and high-performance RF front-end components due to the rapid development of communication technology. The need for extensive frequency bands that can accommodate a range of wireless applications is rising along with the exponential expansion of wireless communication systems. With its high bandwidth and extensive coverage capabilities, centimeter-wave (cmWave) technology has become a crucial component of 6G communication [2, 3]. The realization of 6G's technological potential, which includes holographic displays, high-definition IoT devices, smart and sustainable cities, and immersive digital experiences, is anticipated to be greatly aided by cmWave frequencies [4–7]. By improving communication link dependability and lowering latency, beam-scanning antennas have the potential to completely transform 6G communication. Beam-scanning antennas can reduce interference, path loss, and signal blockage by precisely guiding beams towards specific users or locations, creating more reliable and low-latency communication links [8, 9]. For high-power satellite and radar systems, phased arrays provide the perfect way to achieve beam-scanning [10, 11].

Many techniques have been investigated for main-lobe scanning of phased array antennas, which are extensively utilized in military radars, satellites, and beam-forming applications. Planar array antennas that use adjustable electrical components such as varactor diodes, p-i-n diodes, or mechanical phase shifters are among these techniques [12, 13]. Waveguide phased arrays possess high-power handling capabilities and efficiency, making them a suitable option for high-power radar systems [14, 15]. For wide-angle beam-scanning while preserving performance, some studies suggest mechanical reconfiguration techniques [16, 17]. A 4-element antenna array's beam was controlled by 43 tuning screws in [18], which led to a high level of complexity. Another method in [19] uses rotating dielectric slabs in waveguide arrays. However, the bandwidth and scanning range of this design are limited. Furthermore, it has been demonstrated that adding circulators to transmitting or receiving modules improves beam-scanning capabilities, opening up features such as full duplex communication and boosting wireless communication systems' efficiency [20–22].

The design of a passive electronically scanned array (PESA) system that operates in the 13–17 GHz frequency band and is appropriate for future 6G communication is the main goal of this paper. To achieve precise beam-scanning, the system consists of a 2×2 array of horn antennas that are controlled by electronic reflective phase shifters. For effective signal distribution

© The Author(s), 2026. Published by Cambridge University Press in association with The European Microwave Association.

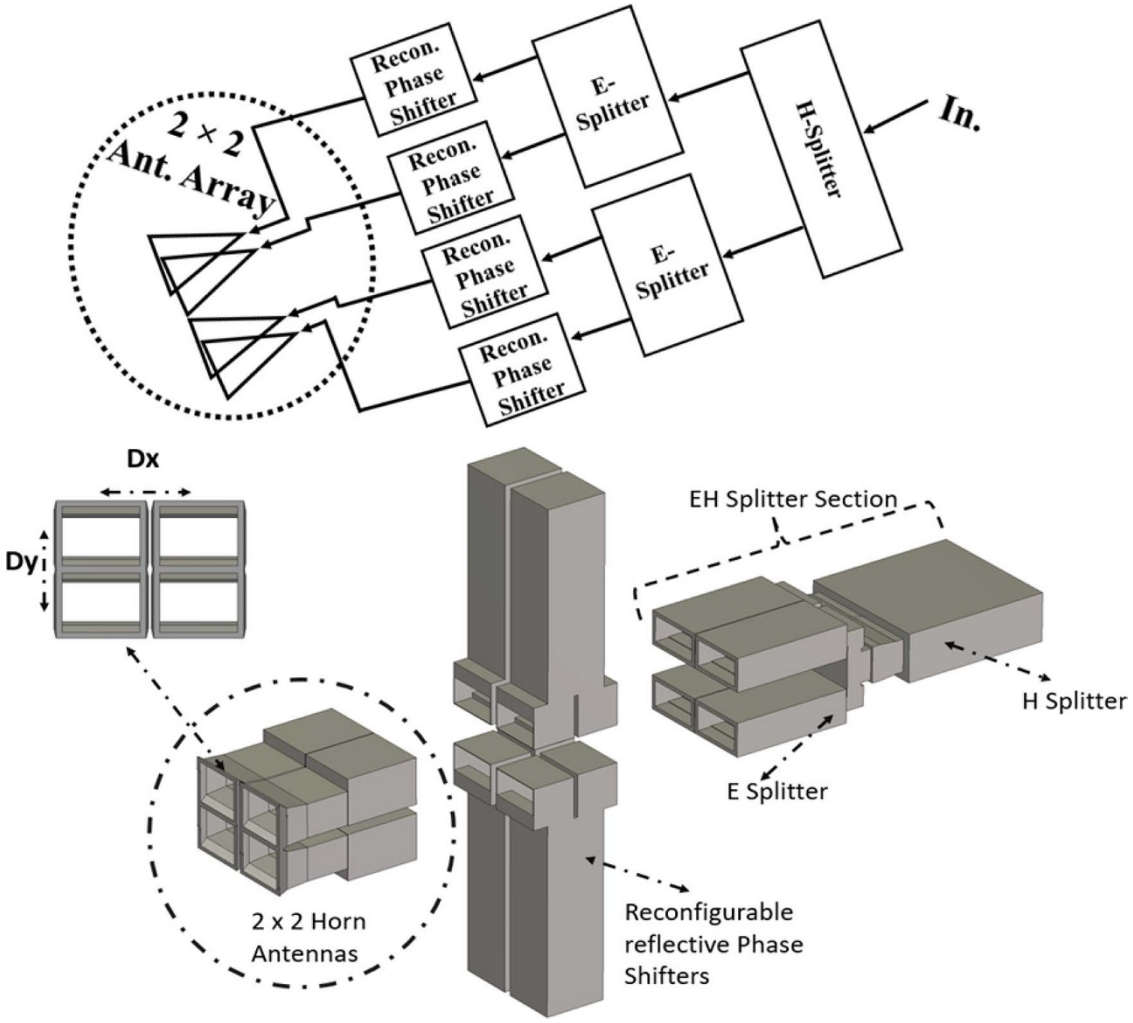


Figure 1. Block diagram and 3D view of the proposed overall PESA.

Table 1. 2 × 2 array output ports' phase profile samples

Φ_x	Φ_y	θ_0	Φ_0	Quadrant	Pos.
−45°	−45°	10°	51°	I	A
130°	−130°	29°	137°	II	B
160°	45°	37°	−141°	III	C
−45°	160°	10°	−75°	IV	D
0°	0°	0°	0°	–	Origin

to the individual horn antennas, the assembly has H-splitter and E-splitter components. Every component is carefully planned and optimized separately before integration. To verify its performance, the complete assembly is then simulated in the time and frequency domains using a full-wave electromagnetic solver. The suggested approach has great potential to advance communication technology, with possible uses in satellite communications, military radars, and Internet of Things devices for distant sensing.

Electronically scanned array configuration

Figure 1 shows the proposed PESA, which consists of four horn antennas fed by a waveguide feeding network. A waveguide reflection-type phase shifter connects each feeding network output to the matching radiating element of the horn antenna array. The feeding network setup has four output ports and one input port, all based on the WR-62 waveguide. In terms of both amplitude and phase, this device evenly distributes the signal at its input port across its four output ports. The pyramidal horns that make up the horn antenna array are intended to provide a good matching level and a steady gain of 8.41 dBi over the intended frequency range. The aperture and flare of the horn are precisely designed to maximize performance. Four separate variable reflect-type phase shifters with digital control comprise the suggested movable short phase shifter module. Due to each phase shifter having its own movable short circuits, the phase shift between the input and output ports may be precisely controlled. The required scanning of the radiation pattern can be achieved by manipulating the relative phase shift between the array elements by varying each short.

It is crucial to note that the design that is being presented is only a proof of concept. Fully automated adjustable short circuits could be used in place of the presented movable short circuits in the device's final real-world implementation. This improvement would include using a motion mechanism that consists of a stepper motor coupled to a long-threaded rod for precise movement and phase difference. A motor shield that is coupled to a microcontroller

https://doi.org/10.1017/S1759078726103304 Published online by Cambridge University Press

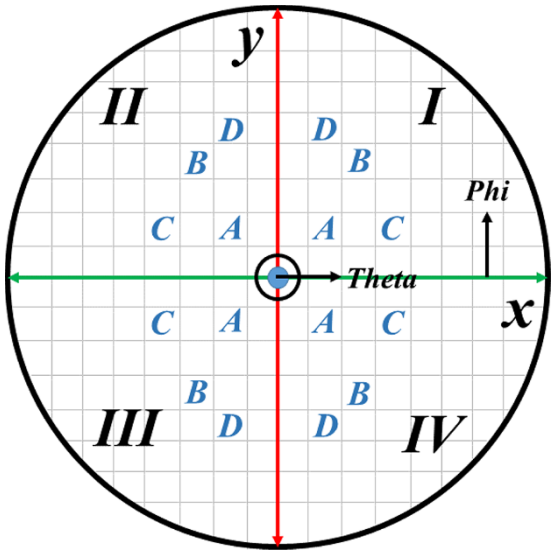


Figure 2. Output beam phase distribution.

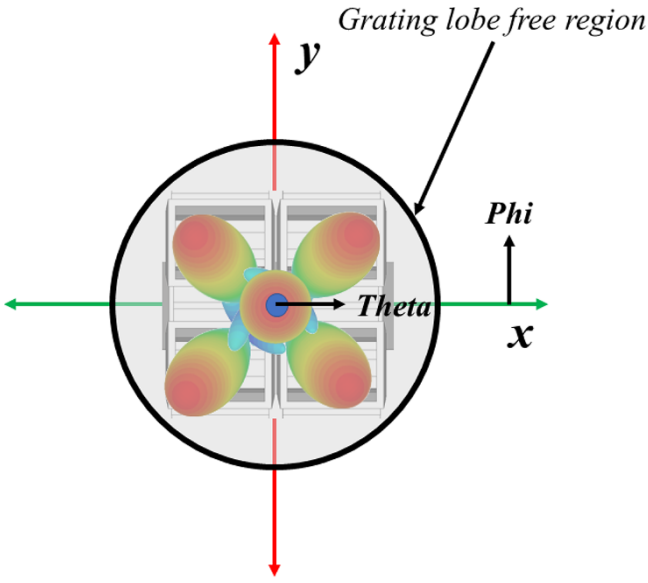


Figure 3. 3D output beam-scanning samples.

would regulate the stepper motor, ensuring accurate and automated short-circuit adjustment.

Electronically scanned array capability

This section explores the proposed beam-scanning capability of the PESA, focusing on a 2 × 2 antenna array configuration. By carefully adjusting element spacing and implementing progressive phase shifts, beam-scanning is accomplished in both the elevation (θ) and azimuth (Φ) planes. The scanning beam angle can be calculated using [9]:

$$\Phi_0 = tan^{-1}\left(\frac{\Phi_x d_x}{\Phi_y d_y}\right) \quad (1)$$

$$\theta_0 = sin^{-1}\sqrt{\left(\frac{\Phi_x}{d_x k}\right)^2 + \left(\frac{\Phi_y}{d_y k}\right)^2} \quad (2)$$

where Φ_x and Φ_y are the progressive phase shifts in the x and y planes, d_x and d_y are the element spacing, and k is the propagation constant in free space.

A 2 × 2 array of horn antennas is excited by a WR-62 rectangular waveguide, allowing for precision beam-scanning across the 13–17 GHz frequency range. The ideal element spacings, represented by $d_x = 18.54$ mm and $d_y = 13.46$ mm, are determined by the waveguide's physical dimensions as well as the geometric properties of the flaring of the horn antennas. Table 1 provides a quantitative evaluation of the scanning performance using the computed output beam samples that were obtained from equations 1 and 2. It is worth mentioning that each beam scanned within every quadrant inherently possesses a complementary counterpart in every quadrant, which is linked to the symmetrical nature of the scanning process. To give a visual representation of the scanning capacity in a 2D polar form and to show the directional features of the antenna array, these results are graphically shown in Figure 2. Additionally, the beam-scanning capacity of the 2 × 2 horn antenna array is explained in Figure 3, which shows beams switched across the origin and the four quadrants. Notably, the visualization also displays areas where scanning can be done successfully without grating lobes appearing, which is an important factor mitigated by optimizing the element spacing.

Beam-scanning network design

The 2 × 2 array requires a reconfigurable feeding network with the same interface, capable of providing uniform amplitudes with varying phases. As a result, each component in the PESA will be designed and optimized separately to verify the functionality of the final network before integration. Each component will be designed based on the WR62 standard for direct integration and testing with a standard waveguide interface.

E–H splitter

The beamforming network illustrated in Figure 1 consists of three primary parts. The E–H splitter, which is the main part, is essential for splitting the input signal. In order to ensure equal magnitude and phase, the input signal is split in half by the H-splitter and then further divided into four by the E-splitters. Figure 4 shows the E–H splitters' internal structure. The E–H splitter's performance is improved by increasing its matching bandwidth with the use of multi-section stepped transformers. The E–H splitter's remarkable matching performance is demonstrated by its S-parameter response, which is shown in Figure 5. Its reflection coefficient remains below −22 dB throughout the 13–17 GHz operational range. Furthermore, over the whole frequency range, the transmission coefficient between the input and output ports is consistently within -6 ± 0.1 dB, indicating low amplitude variation between the outputs.

Reconfigurable phase shifter

The reconfigurable reflective phase shifter, which is essential for beam-scanning activities, is the second main part of the entire assembly. To ensure exact control over the phase shift, a total of four phase shifters will be linked to the four ports of the E-splitters. In order to get precise control over the phase shift, two ports are short-circuited in the E-plane 90° hybrid coupler configuration used to create these phase shifters [23, 24]. Full-wave simulation was used to thoroughly validate the hybrid coupler's performance

https://doi.org/10.1017/S1759078726103304 Published online by Cambridge University Press

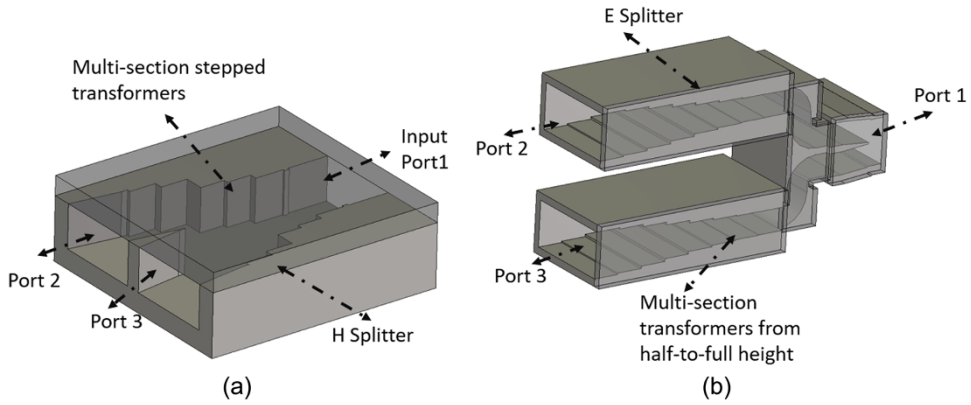


Figure 4. 3D view of the E–H splitter feeding network. (a) H-splitter and (b) E-splitter.

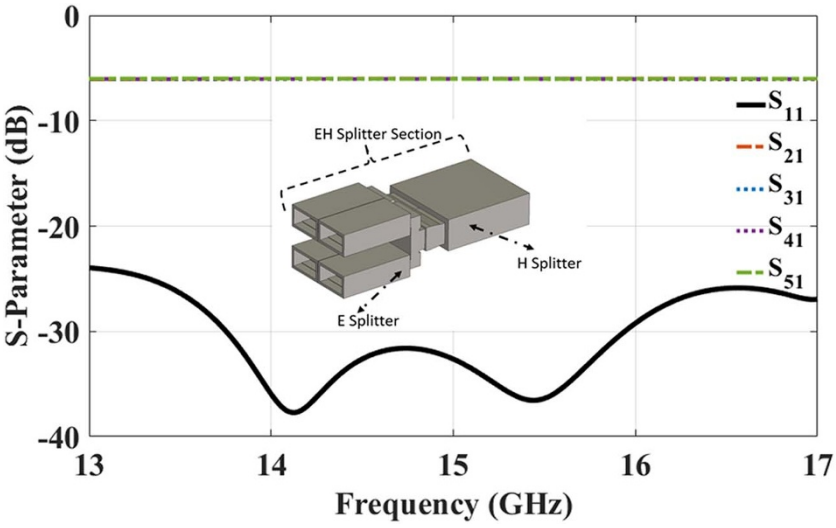


Figure 5. S-parameter response of the proposed E–H splitter.

before the reflecting short circuit was put into practice. As illustrated in Figure 6(a), the suggested hybrid coupler structure uses the E-plane principle and couples via two multi-stepped apertures located in the shared broad wall between the two waveguides. This innovative design guarantees less reflection and improves coupling flatness. Furthermore, the center part of the coupling section is matched to the WR-62 waveguide interface by using a multi-step design of the waveguide main arm, as their effects are demonstrated in Figure 6(b). The matching level is further enhanced by tuning posts beneath the aperture. Both the coupling flatness and the matching level are controlled by carefully selecting the aperture and multi-step dimensions. In addition to guaranteeing accurate phase variation, this design strategy helps the coupler remain compact while still exhibiting a high matching level and enhancing performance. Figure 6(c) displays the wideband 3-dB coupler's S-parameter response. The coupling variation is 3 ± 0.5 dB, with a matching level below −25 dB spanning the 13–17 GHz range.

A movable short to terminate the through and coupled ports can be used to allow full signal transmission to the isolated port. The network will be similar to a crossover where two quadrature hybrid couplers are cascaded, whereas here the signal will combine at the isolated port. A thick aluminum sheet with a sliding piston connected to it and controlled by a stepper motor can be used to vary the phase [25]. Additionally, the movable short can be modified to be a block with RF chokes that act as a bandstop filter based on the impedance of the steps [26]. The RF chokes significantly reduce the RF leakage, which also improves the phase imbalance for the phase shifter. The short with RF chokes is shown in Figure 7.

The reflecting phase shifter's block diagram and 3D view are displayed in Figure 8(a). A phase shift is produced by moving the reflecting short-circuit blocks, which allows the array's beam to be scanned. The reconfigurable phase shifter's S-parameter response is demonstrated in Figure 8(b), where the reflective short circuit is electrically moved to vary the phase at 45° and 90°. The figure shows that the reflection coefficient matching level is better than −18 dB over the whole operating spectrum, even after varying the phase from 45° to 90°. The phase difference vs frequency for a range of phase shifts, from −90° to 90°, is shown in Figure 9. With only a minimal amount of phase variation, the curves show a steady response over the 13–17 GHz frequency range.

Horn antenna

The simplest type of antenna for a rectangular waveguide capable of handling high power is the horn antenna. It also provides

https://doi.org/10.1017/S1759078726103304 Published online by Cambridge University Press

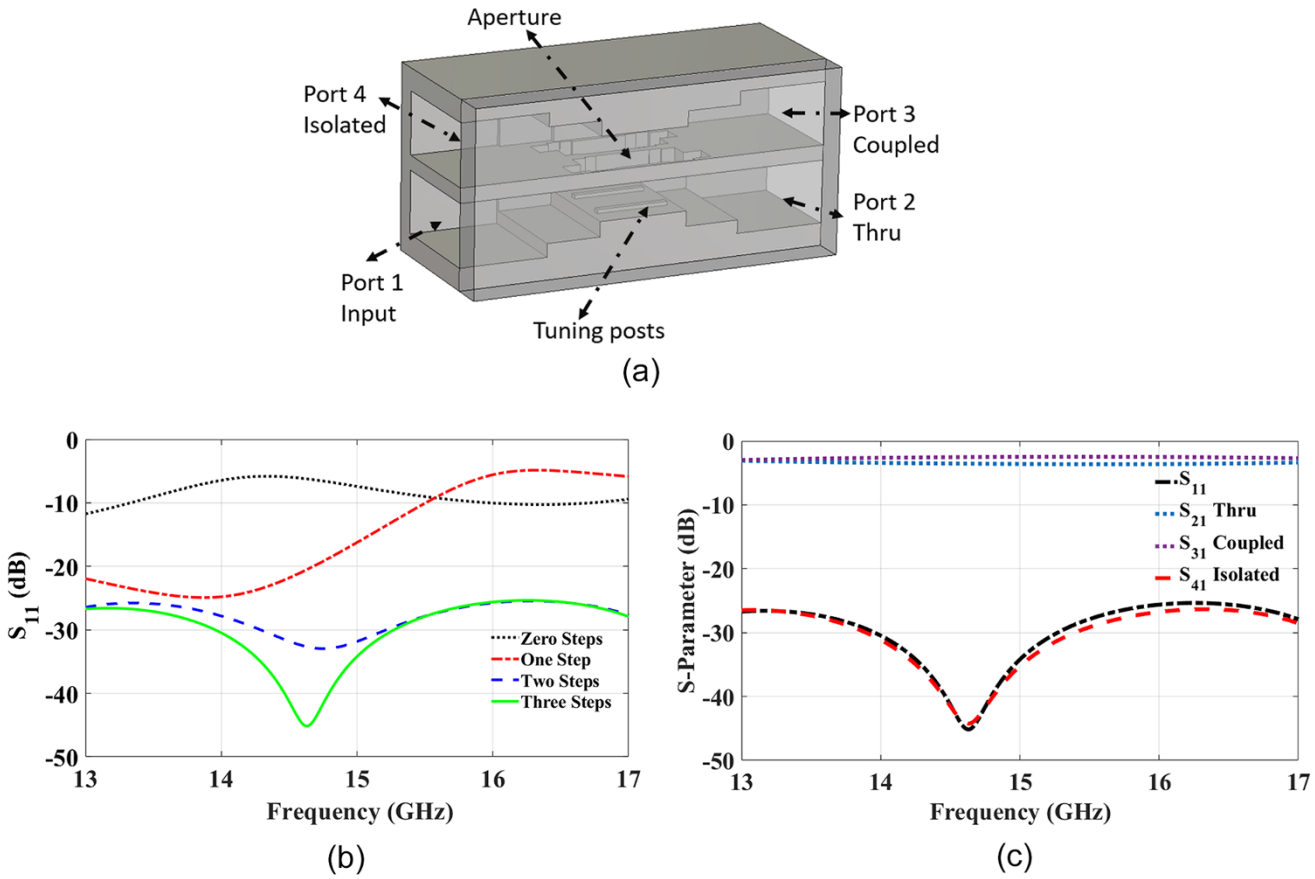


Figure 6. Quadrature hybrid coupler. (a) 3D view. (b) S_{11} using different number of matching steps. (c) Final S-parameter response.

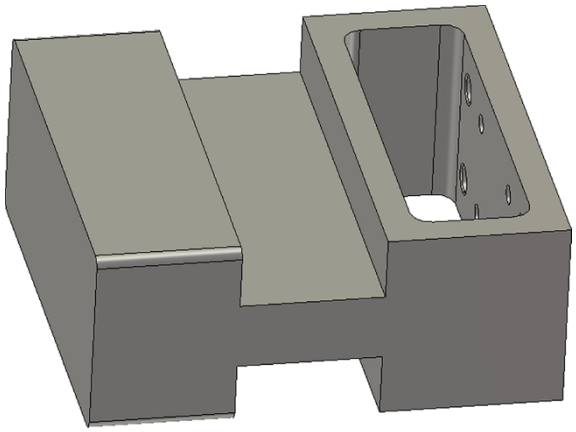


Figure 7. Short with RF chokes.

a directive beam with high gain and a superior matching level for the whole bandwidth. The horn antenna utilized in the 2 × 2 array is shown in Figure 10 along with its matching level, gain, and radiation pattern. The horn antenna has a WR-62 input interface and a minimal flaring to minimize the element spacing in the array and mitigate grating lobes. It also has a reflection coefficient level better than −30 dB and a gain of 8.41 ± 1 dBi over the target bandwidth with a 3-dB beamwidth of 67°.

Beam-scanning antenna array

The pyramidal horn antenna is integrated in a 2 × 2 array and assembled with the previously mentioned reconfigurable network. The array could be switched to scan in all the quadrants and the origin. Figure 11 shows examples of switching radiation patterns to demonstrate the network's flexible scanning capabilities. An outstanding matching level is achieved by optimizing the feeding network and the antennas, which can be sustained at various scanning configurations. This is demonstrated in Figure 12, where even at larger scan angles, a good matching level is maintained and the results are verified in both the time and frequency domains. Similarly, Figure 13 plots the gain against the operating frequency for the various switched beams in both domains. The gain for each of the beams is Origin = 14.6 dBi, Q1 = 14 dBi, Q2 = 12.63 dBi, Q3 = 13.18 dBi, and Q4 = 13.15 dBi at the center frequency. It offers a minimal scan loss, which can be further compensated by the network's capacity to manage high power levels. Some of the previously switched beams are validated using time and frequency domains, as shown in Figure 14, highlighting the effectiveness of the proposed scanning network.

The PESA is capable of handling high power levels due to the utilization of the rectangular waveguide as the guiding medium. Furthermore, a power breakdown occurs due to small gaps inside the structure, causing the air to ionize in the presence of a high voltage difference between the two terminals. In the proposed

https://doi.org/10.1017/S1759078726103304 Published online by Cambridge University Press

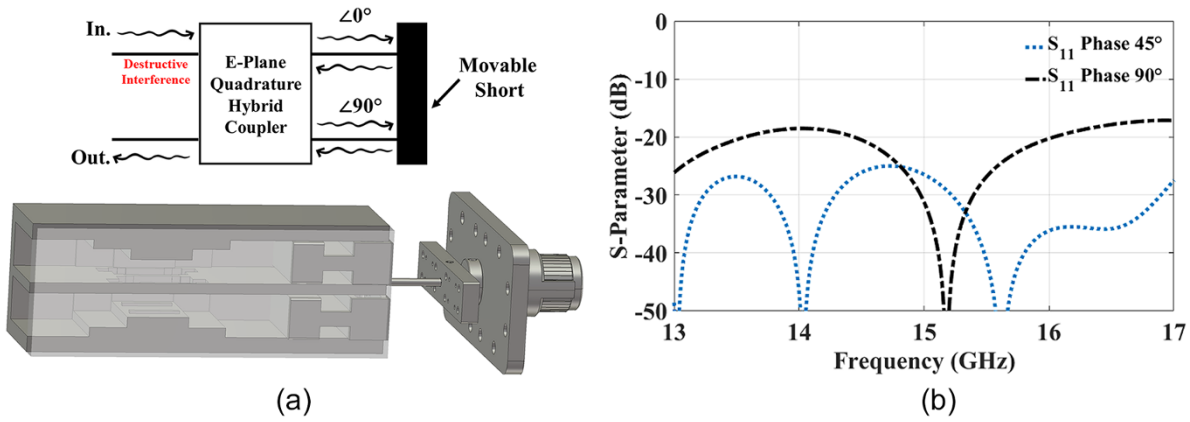


Figure 8. Reconfigurable reflective phase shifter. (a) Block diagram and 3D view. (b) S-parameter response at 45° and 90° by moving the reflective short circuit.

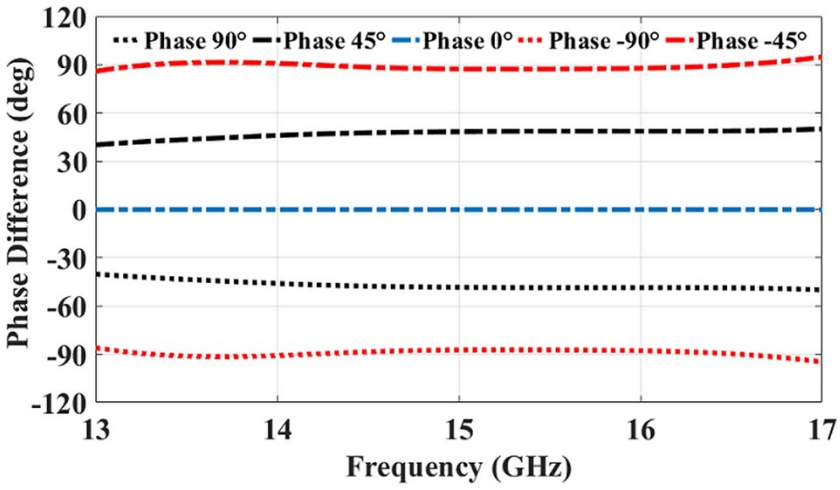
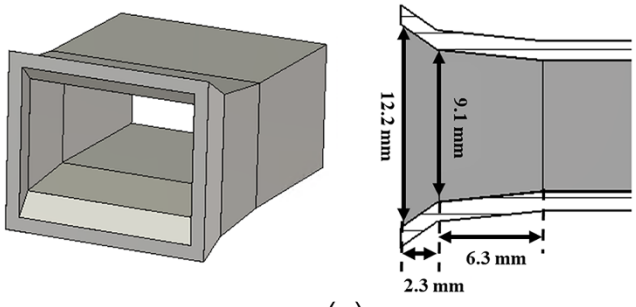


Figure 9. The simulated phase variation of the wideband reflective phase shifter.



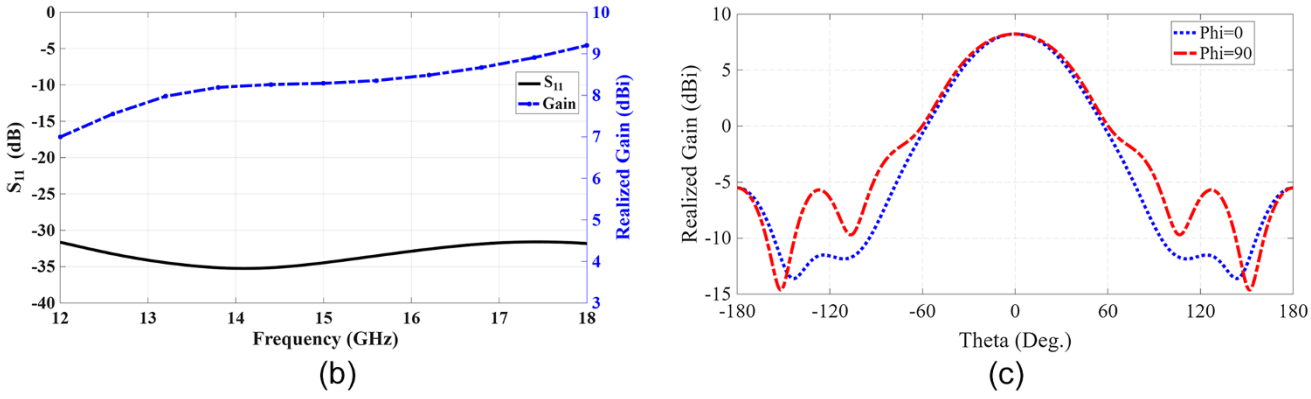


Figure 10. Horn antenna and its frequency response. (a) Structure, (b) S_{11} and gain, and (c) radiation pattern.

https://doi.org/10.1017/S1759078726103304 Published online by Cambridge University Press

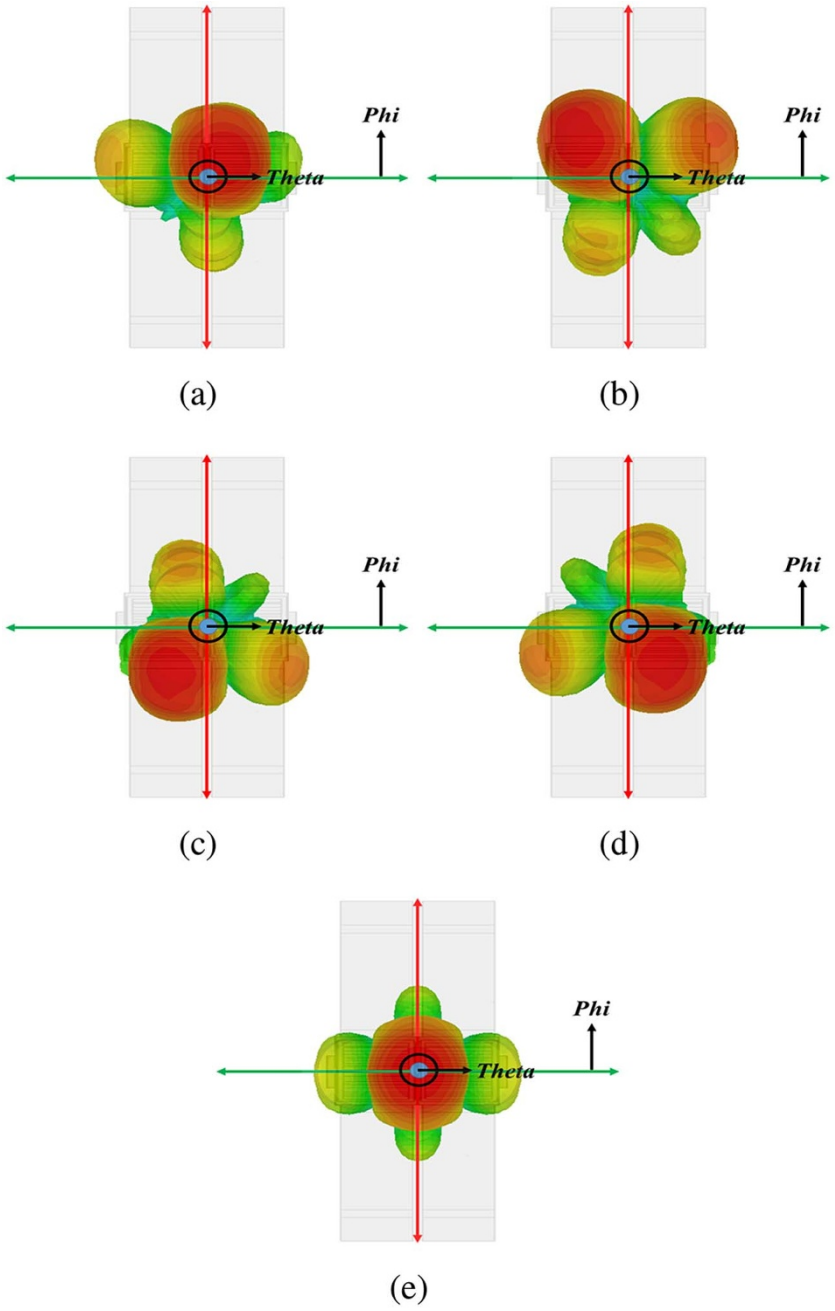


Figure 11. Sample of radiation patterns at (a) Quadrant 1 ($\theta_0 = 9^\circ$, $\Phi_0 = 40^\circ$), (b) Quadrant 2 ($\theta_0 = 22^\circ$, $\Phi_0 = 140^\circ$), (c) Quadrant 3 ($\theta_0 = 18^\circ$, $\Phi_0 = -150^\circ$), (d) Quadrant 4 ($\theta_0 = 18^\circ$, $\Phi_0 = -50^\circ$), and (e) Origin.

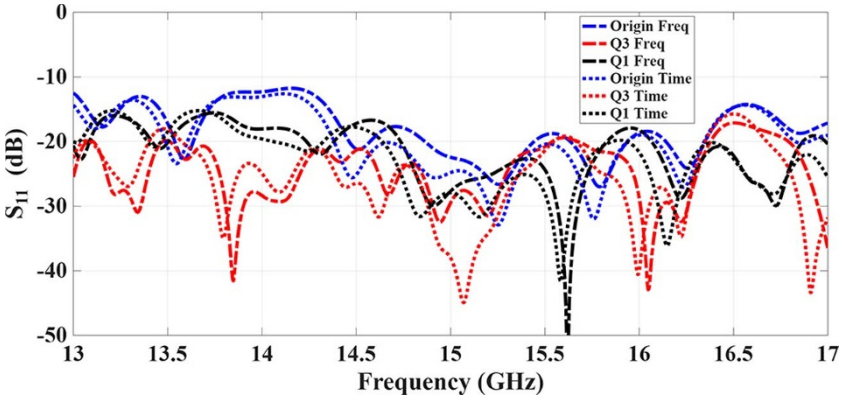


Figure 12. Simulated reflection coefficient using time and frequency domains.

https://doi.org/10.1017/S1759078726103304 Published online by Cambridge University Press

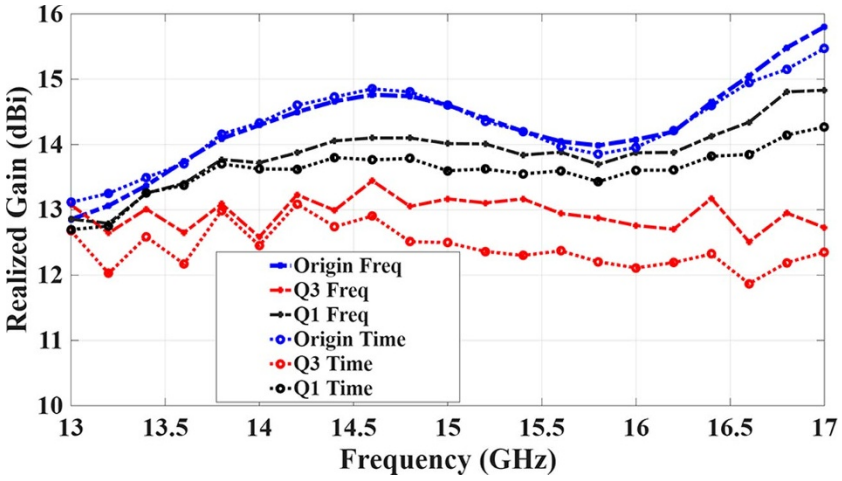


Figure 13. Simulated gain using time and frequency domains.

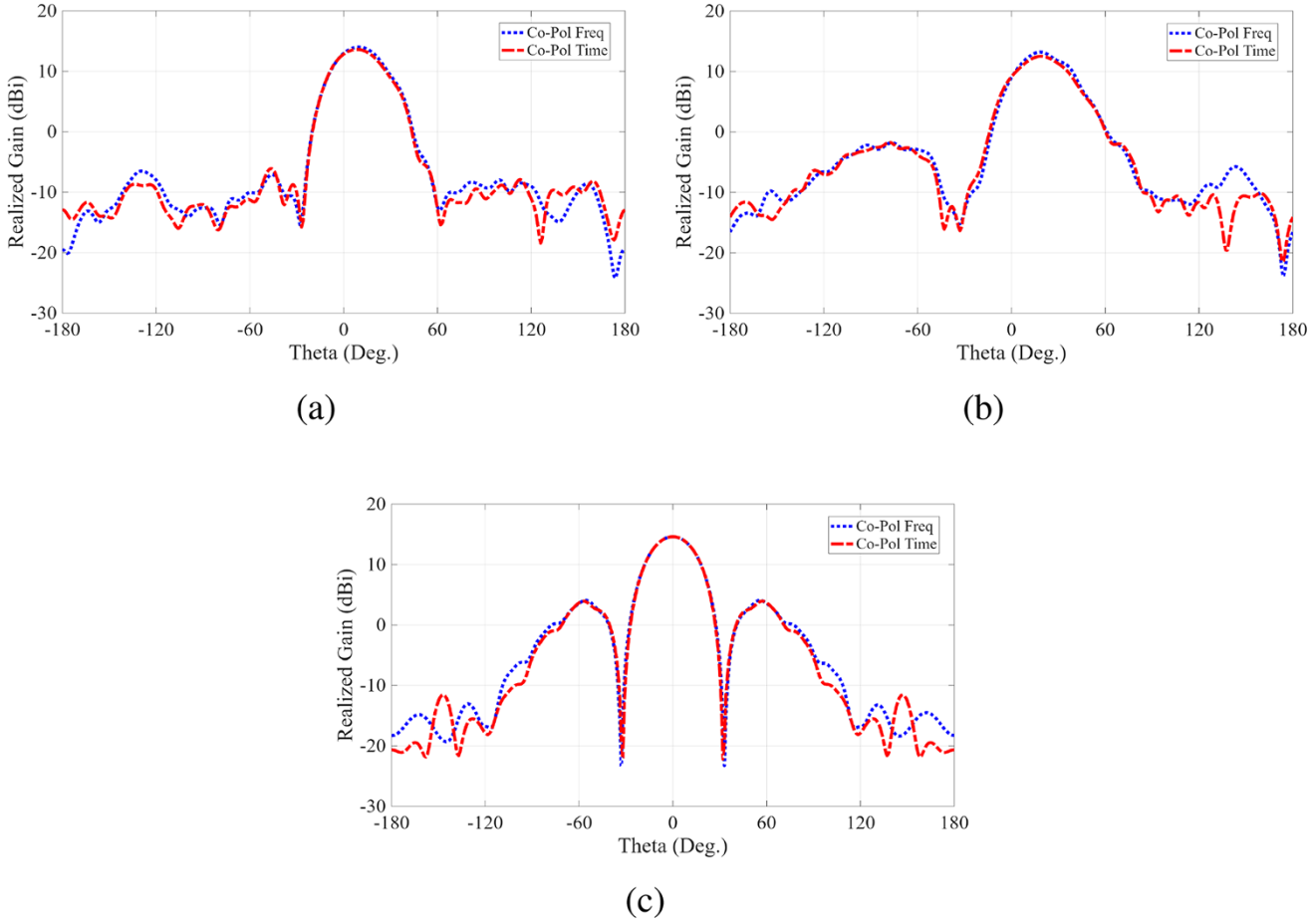


Figure 14. Sample of radiation patterns using frequency and time domains at (a) Quadrant 1 ($\Phi_0 = 40^\circ$), (b) Quadrant 3 ($\Phi_0 = -150^\circ$), and (c) Origin.

beamforming network, the limiting component with the smallest gap is the reconfigurable phase shifter. As a result, corona discharge analysis is conducted using Spark3D for this component to determine the breakdown power. The Paschen curve is plotted in Figure 15, where the breakdown power at atmospheric pressure (1013.25 mbar) is 51 kW, showcasing the high-power capability of the network.

The proposed PESA is compared with others found in the literature in Table 2. Multiple substrate integrated waveguide (SIW) beamforming networks are cascaded in [27] to achieve 2D beam-switching with a low sidelobe level. However, this limits the bandwidth and increases the losses in the network. In [28], a modified groove gap waveguide (GGW) Butler matrix with only two inputs is realized to reduce the complexity and switch the beam

https://doi.org/10.1017/S1759078726103304 Published online by Cambridge University Press

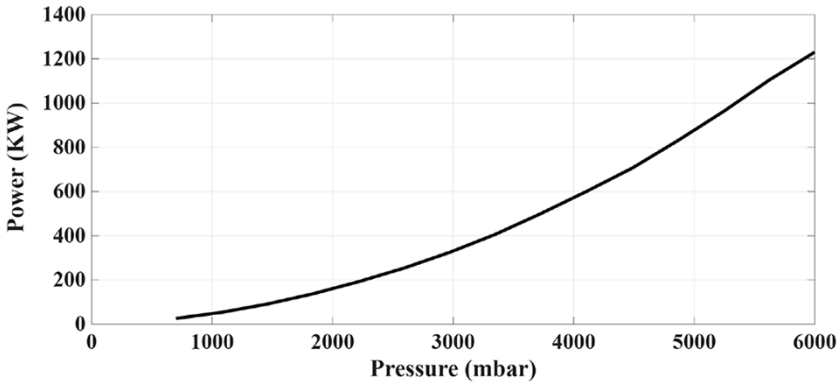


Figure 15. Paschen curve of the reconfigurable phase shifter.

Table 2. Comparison between different PESA in the literature

Reference	Technology	BW%@f_0 (GHz)	Scanning type	Gain (dBi)	Complexity	Power handling
[27]	SIW	3.6%@28	Switched	13.4 ± 0.4	Medium	Low
[28]	GGW	0.7%@94	Switched	N/A	Low	Moderate
[29]	Microstrip	14.3%@28	Continuous	5.6 ± 2	High	Low
[30]	RGW	3.6%@28	Switched	12.9 ± 1.4	Low	Moderate
This work	**WR**	26.6%@15	**Continuous**	14 ± 2	**Medium**	**High**

at the W-band. Similarly, the network is limited in bandwidth and scan coverage. A microstrip Butler matrix that utilized reconfigurable liquid crystal phase shifters to scan the beam continuously in [29]. However, this increases the complexity and the losses significantly of the output signal. A ridge gap waveguide (RGW) multilayer Butler matrix is proposed in [30] that improves the scanning coverage. However, the network has a considerable size of $11.3\lambda \times 11.2\lambda$ and a limited bandwidth.

This PESA provides a straightforward reconfigurable network with superior scanning coverage and matching level. Additionally, the network can withstand high power levels due to the rectangular waveguide guiding medium and the lack of small gaps inside the structure [31, 32]. Using an antenna element with a broader radiation pattern beamwidth to cover the majority of the scanning range could help reduce the scanning loss. A half-height structure and smaller antenna elements might also be used to lower the grating lobe level by decreasing the spacing. However, this would result in a reduction in power handling capacity, gain, and matching level.

Conclusion

In this work, a PESA utilizing reflective phase shifters has been discussed in detail for future 6G applications. Four digitally controlled variable reflect-type phase shifters, each built with a 90° hybrid coupler with a movable short-circuit, are integrated with a 2×2 horn antenna array. Outstanding performance has been demonstrated by the simulation results for the whole PESA, which show continuous main-lobe scanning in the azimuth and elevation planes. The suggested work may be appropriate for complex antenna systems and can be utilized in radar systems and beam-scanning next-generation satellite communications.

Competing interests. The authors declare none.

References

1. **Ali MMM, Shady MO, Sifat SM, Hettak K, Talbi L and Wu K** (2025) Centimeter-wave electronically scanned array for future 6G applications. In *Proceedings of the 19th European Conference on Antennas and Propagation (EuCAP)*. Stockholm, Sweden, pp. 1–5. https://doi.org/10.23919/EuCAP63536.2025.10999658
2. **Adeogun R, Berardinelli G, Mogensen PE, Rodriguez I and Razzaghpour M** (2020) Towards 6G in-X subnetworks with sub-millisecond communication cycles and extreme reliability. *IEEE Access* **8**, 10172–110188.
3. **Ericsson White Paper** (2022) 6G connection a cyber-physical world, GFTL-20. 001402.
4. **Akyildiz IF, Kak A and Nie S** (2020) 6G and beyond: The future of wireless communications systems. *IEEE Access* **8**, 133995–134030.
5. **Aliouane MA, Conrat JM, Cousin JC and Begaud X** (2022) Material reflection measurements in centimeter and millimeter wave ranges for 6G wireless communications. In *Proceedings of the Joint European Conference on Networks and Communications & 6G Summit (EuCNC/6G Summit)*. Grenoble, France, pp. 43–48.
6. **Wu Y, Wang Y, Huang J, Wang CX and Huang C** (2022) A weighted random forest based positioning algorithm for 6G indoor communications. In *Proceedings of the IEEE 96th Vehicular Technology Conference (VTC)*. London, United Kingdom, pp. 1–6.
7. **Ratchagar NP, KS A and Agrawal T** (2023) Convergent technologies in 6G: Communication, and sensing, positioning. In *Proceedings of the International Conference on Power Energy, Environment & Intelligent Control (PEEIC)*. Greater Noida, India, pp. 956–960.
8. **Shady MO and Kishk AA** (2023) Compact 4×4 multilayer Butler matrix with four-slot array. *IEEE Transactions on Microwave Theory and Techniques* **72**(6), 3522–3529.
9. **Ali MMM and Sebak AR** (2018) 2-D scanning magnetoelectric dipole antenna array fed by RGW Butler matrix. *IEEE Transactions on Antennas and Propagation* **66**(11), 6313–6321.
10. **Yu Y, Hong W, Jiang ZH and Zhang H** (2020) A hybrid radar system with a phased transmitting array and a digital beamforming receiving array. *IEEE Transactions on Antennas and Propagation* **69**(4), 1970–1981.
11. **Shin D, Kim CY, Kang DW and Rebeiz GM** (2013) A high-power packaged four-element X-Band phased-array transmitter in 0.13-μm CMOS

https://doi.org/10.1017/S1759078726103304 Published online by Cambridge University Press

for radar and communication systems. *IEEE Transactions on Microwave Theory and Techniques* **61**(8), 3060–3071.
12. **Xiao S, Zheng C, Li M, Xiong J and Wang BZ** (2015) Varactor-loaded pattern reconfigurable array for wide-angle scanning with low gain fluctuation. *IEEE Transactions on Antennas and Propagation* **63**(5), 2364–2369.
13. **Huang C, Pan W, Ma X, Zhao B, Cui J and Luo X** (2015) Using reconfigurable transmitarray to achieve beam-steering and polarization manipulation applications. *IEEE Transactions on Antennas and Propagation* **63**(11), 4801–4810.
14. **Courtney CC and Baum CE** (2000) The coaxial beam-rotating antenna (COBRA): Theory of operation and measured performance. *IEEE Transactions on Antennas and Propagation* **48**(2), 299–309.
15. **Yu LZ, Yuan CW, He JT and Zhang Q** (2018) Beam steerable array antenna based on rectangular waveguide for high-power microwave applications. *IEEE Transactions on Plasma science* **47**(1), 535–541.
16. **Polo-López L, luis Masa-Campos J, Muriel-Barrado AT, Sanchez-Olivares P, Garcia-Marin E, Córcoles J and Ruiz-Cruz JA** (2020) Mechanically reconfigurable linear phased array antenna based on single-block waveguide reflective phase shifters with tuning screws. *IEEE Access* **8**, 113487–113497.
17. **Jouade A, Himdi M, Chauloux A and Colombel F** (2017) Mechanically pattern-reconfigurable bended horn antenna for high-power applications. *IEEE Antennas and Wireless Propagation Letters* **16**, 457–460.
18. **Sanchez-Olivares P, Masa-Campos JL, Muriel-Barrado AT, Villena-Medina R and Fernandez-Romero GM** (2018) Mechanically reconfigurable linear array antenna fed by a tunable corporate waveguide network with tuning screws. *IEEE Antennas and Wireless Propagation Letters* **17**(8), 1430–1434.
19. **Ghasemi A and Laurin J-J** (2019) A continuous beam steering slotted waveguide antenna using rotating dielectric slabs. *IEEE Transactions on Antennas and Propagations* **67**(10), 6362–6370.
20. **Shams SI, Sifat SM, Elsaadany M, Gagnon G and Kishk AA** (2021) Systematic design procedure for Y-junction circulator based on ridge gap waveguide technology. *IEEE Transactions on Microwave Theory and Techniques* **69**(4), 2165–2177.
21. **Sifat SM, Shams SI and Kishk AA** (2023) Millimeter-wave ferrite circulator integrated on gap waveguide technology. *IEEE Microwave and Wireless Components Letters* **33**(8), 1151–1154.
22. **Ali MMM, Elsaadany M, Shams SI and Wu K** (2024) On the design of broadband asymmetric Y-junction ferrite circulator for 60-GHz inter-satellite communication. *IEEE Transactions on Microwave Theory and Techniques* **72**(2), 892–902.
23. **Cano JL, Ceccato G, Fernandez T, Mediavilla A and Perregrini L** (2022) An ultra-compact full-band waveguide quadrature hybrid coupler. *IEEE Microwave and Wireless Components Letters* **32**(1), 9–12.
24. **Shady MO, Ali MMM and Kishk AA** (2024) Ultra-wideband millimeter-wave tight and loose microstrip aperture couplers. *IEEE Microwave and Wireless Technology Letters* **34**(9), 1071–1074.
25. **Popela M, Simon O and Lacik J** (2023) Electronically controlled waveguide phase shifter for high power applications. In *Proceedings of the IEEE 33rd International Conference Radioelektronika*. Pardubice, Czech Republic, pp. 1–4.
26. **Choi J-H and Kim Y-H** (2016) A high-power waveguide phase shifter with periodic RF chokes for subgigawatt nanopulse transmission. *IEEE Transactions on Plasma Science* **44**(10), 2307–2313.
27. **Lian J-W, Ban Y-L, Zhu J-Q, Guo J and Chen Z** (2019) Planar 2-D scanning SIW Multibeam array With low sidelobe level for millimeter-wave applications. *IEEE Transactions on Antennas and Propagation* **67**(7), 4570–4578.
28. **Tamayo-Domínguez A, Fernández-González J-M and Sierra-Castañer M** (2020) 3-D-printed modified Butler matrix based on gap waveguide at W-band for monopulse radar. *IEEE Transactions on Microwave Theory and Techniques* **68**(3), 926–938.
29. **Wang D, Polat E, Tesmer H, Maune H and Jakoby R** (2022) Switched and steered beam end-fire antenna array fed by wideband via-less Butler matrix and tunable phase shifters based on liquid crystal technology. *IEEE Transactions on Antennas and Propagation* **70**(7), 5383–5392.
30. **Geng C, Lian J-W and Ding D** (2025) Millimeter-wave highly efficient E-plane ridge gap waveguide Butler matrix for wide-angle endfire multi-beam antenna applications. *IEEE Transactions on Microwave Theory and Techniques* **73**(8), 5096–5107.
31. **Ali MMM, Sifat SM, Elsaadany M, Shams SI and Wu K** (2024) Innovative development approach for a high-power 8-way coaxial radial combiner. In *Proceedings of the IEEE MTT-S International Microwave Symposium Dig.* Washington, DC, USA, pp. 788–791.
32. **Ali MMM, Shady MO, Elsaadany M, Shams SI, Gagnon G and Ke W** (2024) Research and development of WRD600: Innovations in high-power double-ridge waveguide combiners for ultra-wideband applications. In *Proceedings of the IEEE MTT-S International Microwave Symposium Dig.* Washington, DC, USA, pp. 26–29.

https://doi.org/10.1017/S1759078726103304 Published online by Cambridge University Press